A Planar Dual-Polarized Phased Array with Broad Bandwidth and Quasi End-Fire Radiation for 5G Mobile Handsets

Ojaroudi Parchin, Naser; Zhang, Jin; A. Abd-Alhameed, Raed; Pedersen, Gert Frølund; Zhang, Shuai

Published in:
I E E E Transactions on Antennas and Propagation

DOI (link to publication from Publisher):
10.1109/TAP.2021.3069501

Publication date:
2021

Document Version
Accepted author manuscript, peer reviewed version

A Planar Dual-Polarized Phased Array with Broad Bandwidth and Quasi End-Fire Radiation for 5G Mobile Handsets

Naser Ojaroudi Parchin, *Member, IEEE,* Jin Zhang, Raed A. Abd-Alhameed, *Senior Member, IEEE,* Gert Frølund Pedersen, *Senior Member, IEEE*, and Shuai Zhang, *Senior Member, IEEE*,

***Abstract*—A planar dual-polarized phased array is proposed for 5G cellular communications. The array has the properties of dual-polarization, wideband and quasi end-fire radiation, which is printed on one side of a single-layer substrate. The design contains two 8-element sub-arrays including horizontally polarized end-fire dipole antennas and vertically polarized end-fire periodic slot antennas, employed on the PCB ground plane of the 5G mobile platform. Both sub-arrays provide wide bandwidth to cover 28 and 38 GHz (promising 5G candidate bands). The -10 dB impedance bandwidth of the proposed CPW-fed dipole and slot antennas are 26.5-39.5 GHz and 27.1-45.5 GHz, respectively. Moreover, for -6 dB impedance bandwidth, these values could be more than 20 GHz (24.4-46.4 GHz for the dipole antenna) and 70 GHz (22.3-95 GHz for the slot antenna). The fundamental characteristics of the proposed dual-polarized 5G antenna array in terms of the impedance bandwidth, realized gain, polarization, radiation pattern, and beam steering are investigated and good results are obtained. The clearance of the proposed dual-polarized 5G antenna array is less than 4.5 mm which is sufficient for cellular applications.**

***Index Terms*—5G, broadband communications, end-fire antenna, dual polarization, handset antenna.**

I. Introduction

Compared with existing networks, the next generation (5G) network is expected to provide significantly improved performance such as increased data rates due to the wider bandwidth it employs in millimeter-wave (mm-Wave) spectrum [1]-[2]. Different from the design of antennas for 4G, increasing the operating frequency would bring some challenges and considerations in the antenna design concepts for the 5G handset devices which need new techniques [3]-[5].

This work is partially supported by the InnovationsFonden project of Reconfigurable Arrays for Next Generation Efficiency (RANGE), AAU Young Talent Program, and European Union's Horizon 2020 research and innovation programme under grant agreement H2020-MSCA-ITN-2016SECRET-722424. (Corresponding author: Shuai Zhang)

N.O. Parchin, J. Zhang, G.F. Pedersen and S. Zhang are with the Antennas, Propagation, and Millimeter-Wave Systems (APMS) Section, Aalborg University, Aalborg 9220, Denmark. N.O. Parchin is also with Faculty of Engineering and Informatics, University of Bradford, Bradford BD7 1DP, U.K. (e-mails: N.OjaroudiParchin@bradford.ac.uk; jzhang@es.aau.dk; gfp@es.aau.dk; and sz@es.aau.dk;).

R.A. Abd-Alhameed is with Faculty of Engineering and Informatics, University of Bradford, Bradford BD7 1DP, U.K (e-mail: R.A.A.Abd@bradford.ac.uk).

Since the mobile terminals are randomly oriented compared with the base stations, antenna arrays with dual-polarization are very desirable in future 5G millimeter-wave (mm-wave) cellular communications. Furthermore, dual-polarized antennas are possible to work as MIMO antennas to double the channel capacity [6]. Several designs of dual-polarized mm-wave antenna arrays have been reported in the [7]-[9]. However, few works with end-fire radiation patterns are introduced for mm-wave 5G mobile terminals [10]-[15]. In [10], a dual-polarized end-fire antenna array with a ring-slot is designed on a smartphone metal-frame for 28 GHz 5G applications. The antenna has a uni-planar configuration and exhibits narrow bandwidth (less than 1 GHz). Other designs of 28 GHz phased array with narrow bandwidth and complex design configuration are presented in [11]-[12]. In [13]-[15], different designs of 60 GHz phased arrays with polarization diversity are reported for 5G smartphones. However, the antenna elements are formed in the multi-layer package schematic which needs careful consideration in terms of fabrication and feeding. Besides, these designs only cover 60 GHz, but not 28 or 38 GHz 5G bands.

Apart from the dual-polarization function, the bandwidth and size of the employed radiators would be challenging issues for future cellphone devices [16]-[17]. A wideband dual-polarized antenna end-fire radiation is proposed in [18] for mm-Wave MIMO terminals. However, the antenna size is big and is mainly designed for 36 GHz band. Another example of the wideband dual-polarized end-fire antenna is proposed in [19]. The antenna has been fed using a substrate integrated waveguide (SIW) feeding technique. As explained above, all these antennas either provide narrow impedance bandwidth or occupy large clearance with complex feeding structures. Inevitably, these antennas will encounter some trouble and inconvenience when the space for antennas is limited and also confront difficulty in fabrication which can increase the fabrication cost. This is mainly due to the required vertical-polarization function of the designs, which is challenging to achieve in a thin planar structure [20].

To overcome these drawbacks, we present here a compact planar dual-polarized antenna array with simple design procedure, quasi-end-fire radiation, and wideband for the 5G handset applications. To our best knowledge, this is the first time that the dual-polarized end-fire function is realized with a

planar structure printed on one side of a single-layer substrate, a unique feature that none of the reported designs have. A coplanar-waveguide (CPW) feeding technique is employed on the same layer of the antenna elements which is easy to fabricate and integration and can achieve wideband impedance matching [21]. Therefore, compared with the reported designs, the proposed antenna is low-cost and easy to fabricate. In the proposed configuration, eight elements of CPW-fed periodic slot antennas are etched on top of the mobile-phone PCB to form a vertically-polarized sub-array. In addition, another set of the linear sub-array including CPW-fed dipole radiators with horizontal end-fire radiation modes is used in the same area in the way of each radiator is employed between the periodic slot resonators. Since the slot antennas and dipole antennas are complementary elements, they could provide different (vertical/horizontal) polarization modes. Unlike most of the reported dual-polarized designs, the employed sub-arrays provide very wide bandwidth to cover the 5G bands of 28 GHz and 38 GHz. In addition, the overall dimension of the proposed antenna array is highly compact in size (or with small clearance, less than 4.5 mm) and suitable for 5G cellphone platforms.

This paper is structured as follows: Schematic and design details of the proposed dual-polarized array are described in Section II. Section III will discuss the simulation results of the dual-polarized phased array in terms of its fundamental characteristics. The measurement results are provided and discussed in Section IV. The last Section will conclude this study.

II. Antenna Configuration

Figure 1 displays the schematic of the proposed wideband dual-polarized 5G antenna array. As illustrated, it is composed of two end-fire sub-arrays including a vertically polarized periodic slot sub-array and a horizontally polarized dipole sub-array, which are employed in the top side of a smartphone PCB. Unlike the reported designs, in the proposed dual-polarized smartphone array, the sub-arrays and ground plane have been etched on the same copper layer to ease of integration with the circuits of the 5G smartphone.

The clearance of the proposed dual-polarized array can be reduced to 4.4 mm (see L_a in Fig. 1 (b)). A Rogers 5870 substrate 1.575 mm thickness is used as the PCB substrate with the permittivity of 2.3. As shown in Fig. 1 (c), the antenna element of the horizontally polarized sub-array is composed of a driven element, an L-shaped feeding line, and the reflector ground plane. The feeding line can act as a balun for converting the unbalanced signal to the balanced signal, namely from the dominant mode of coplanar waveguide to the coplanar stripline mode [22]. It is an antenna producing end-fire radiation with horizontal polarization. The antenna element of the vertically polarized sub-array in Fig. 1 (d) is a periodic folded slot as the main framework with multiple connected rectangular slots with different sizes which act as resonators at different frequencies for bandwidth enhancement. The values of parameters for the proposed dual-polarized array are specified in Table I.

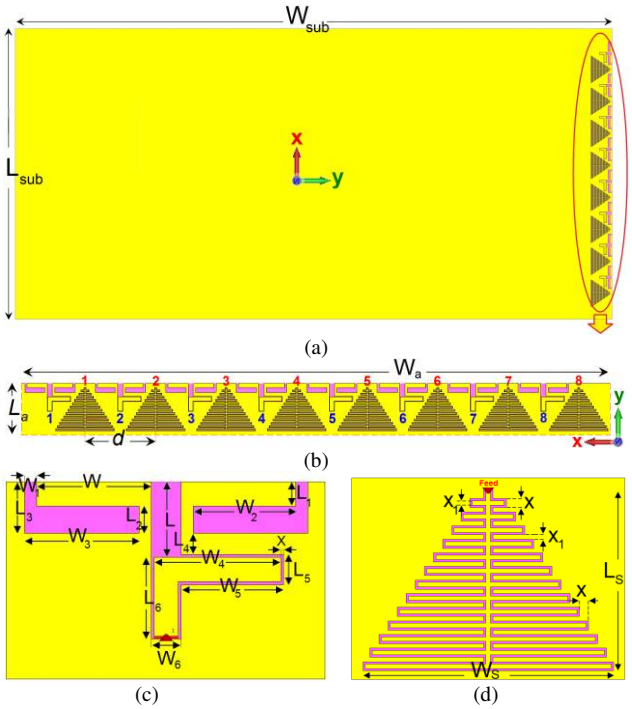

Fig. 1. Array antenna configurations: (a) mobile-terminal PCB, (b) the CPW-fed periodic slot sub-array and the CPW-fed dipole sub-array, (c) dipole array element, and (d) periodic slot array element.

TABLE I
Parameter Values of the Proposed Design

Parameter	W_{sub}	L_{sub}	h_{sub}	W_a	L_a	X
Value (mm)	120	65	1.575	54.6	4.4	0.2
Parameter	W_S	L_S	W	L	W_1	L_1
Value (mm)	5.5	4	1.9	1.25	0.2	0.4
Parameter	W_2	L_2	W_3	L_3	W_4	L_4
Value (mm)	1.7	0.45	1.9	0.85	2.1	0.35
Parameter	W_5	L_5	W_6	L_6	d	X_1
Value (mm)	1.7	0.5	0.5	1.35	6.6	0.1

Figure 2 (a) plots a system architecture in which the dual-polarized antenna array can be applied. In order to have beam-steering function within wide scanning angles, it is required to employ 1×N configuration for the proposed sub-arrays. This might increase the complexity of the system but would improve the performance of the array which is suitable for point to point communications. The feeding network and beam steering function can be accomplished by employing cheap phase shifters, such as HMC933LP4E [24]. In addition, by using a switch, such as SP3T AlGaAs [25], the selection among the sub-arrays to excite the required polarization can be easily achieved. However, it is also possible to excite both sub-arrays simultaneously. In this case, two excitations are required. The broadband antenna elements of the smartphone should be considered as part of the front-end module and can be located close to the 5G RF transceiver and link directly to the radiofrequency integrated circuit (RFIC) chip [25].

The proposed dual-polarized array design can be easily integrated with the RFIC chip of the mobile-phones. Figure 2 (b) shows one possible feeding technique with strip-line

feeding method for the proposed array using a multi-layer substrate. The strip-lines are connected to 50-Ohm waveguide ports employed on a pair of metal walls connected together. It should be noted that the proposed feeding technique is employed without any change in the configuration of the elements or the parameters of the design substrate. According to some investigation, the proposed feeding technique could exhibit sufficient performances in terms of S-parameter and radiation beams, similar to the main design.

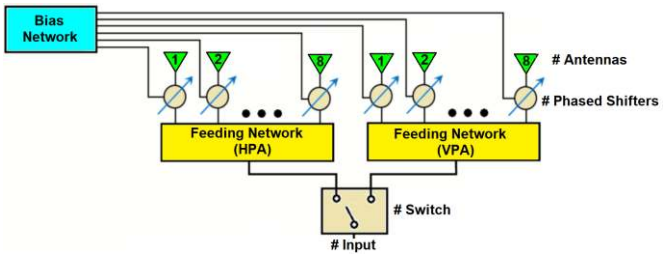

(a)

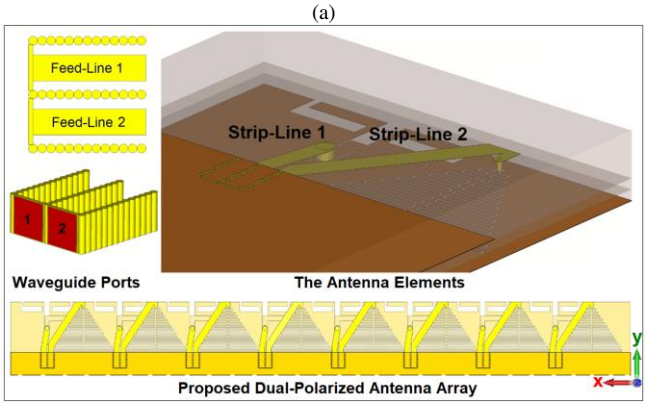

(b)

Fig. 2. (a) Phased array network architecture and (b) one possible feeding technique in practice.

III. Simulation Results

A. Horizontally Polarized End-fire Dipole Antenna Sub-array

Figure 3 (a) illustrates the configuration of the 1×8 dipole antenna sub-array. The distance between the antenna elements (center-to-center) is 4.9 mm. As seen, like other CPW-fed antennas, the antenna feed-line is realized with the balun structure on the same copper layer. The antenna configuration consists of driven elements as radiators and the ground plane as the reflector. The calculated S-parameters of the sub-array are depicted in Fig. 3 (b). The proposed sub-array achieves a broad bandwidth of 26.5-39.5 GHz for S_{11}≤-10 dB and 24.4-46.4 GHz for S_{11}≤-6 dB, which covers the 5G bands (28/38 GHz). Besides, low mutual couplings have been obtained between the radiation elements.

The simulated fundamental radiation properties including the directivity, radiation, and total efficiencies of the array beams over the scanning angles at the center frequency (33 GHz) are represented in Fig. 4. As seen, the proposed dipole antenna array achieves more than -0.5 dB (90%) radiation and total efficiencies over the scanning angles of 0°~75°. It is evident that the array provides sufficient directivity levels varying from 8.5 to 12 dBi. In addition, the sub-array provides a good end-fire realized gain at different angles.

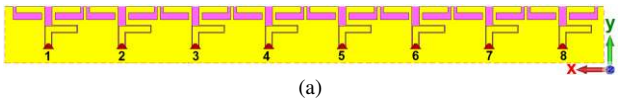

(a)

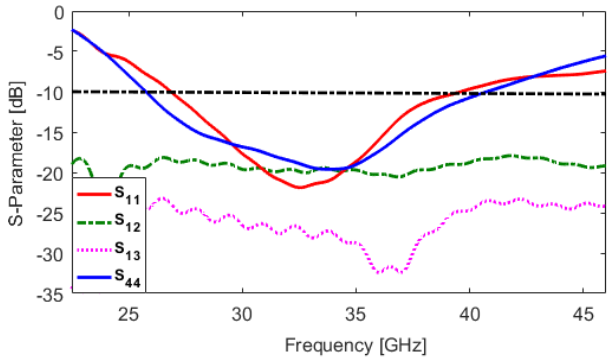

(b)

Fig. 3. (a) Configuration and (b) S parameters of the dipole antenna array.

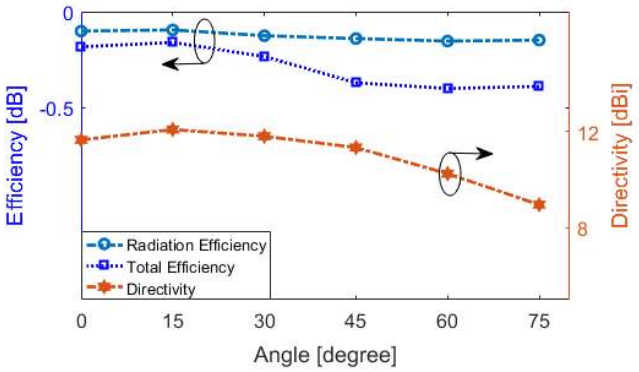

Fig. 4. Radiation properties of the dipole sub-array over its scanning angles at 33 GHz.

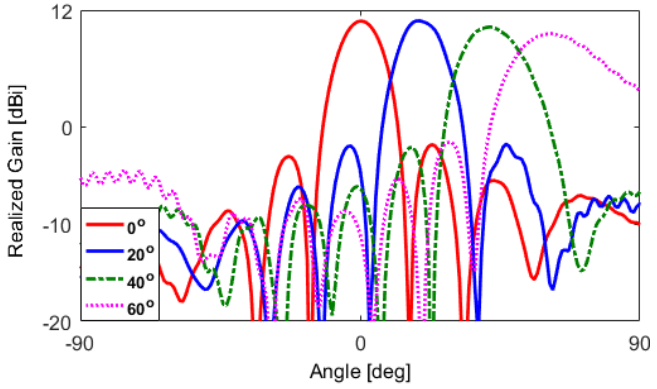

(a)

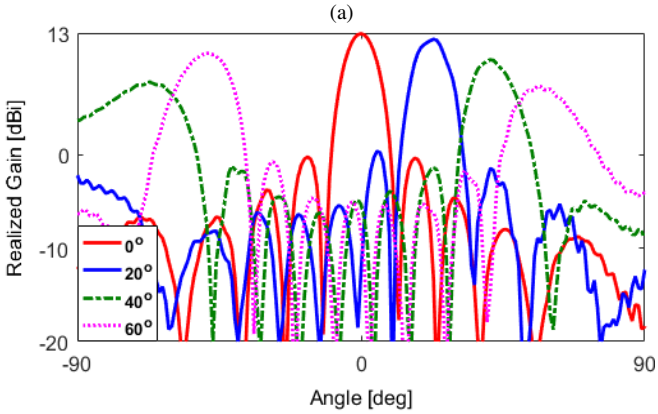

(b)

Fig. 5. Realized gain of the sub-array at (a) 28 GHz and (b) 38 GHz.

The cartesian realized gain results of the horizontally polarized sub-array at 28 and 38 GHz are represented in Fig. 5. For the 28 GHz, the antenna gain is almost constant and more than 10 dBi for the scanning range of 0°~60°. However, as the distance between the elements is larger than λ/2, it is difficult to achieve high gain levels at the large scanning angles. It should be noticed that according to the 3rd generation partnership project (3GPP), the equivalent isotropically radiated power (EIRP) requirements at 38 GHz is lower than those at 28 GHz. The reason is because the existence of the grating lobe at 38 GHz is expected if the array inter-element distance is determined by 28 GHz or lower frequencies. In addition, as long as the gain (or EIRP) aligns the requirement, the user equipment (UE) doesn't need to acquire the grating lobe levels until now [26].

B. Vertically Polarized Periodic Slot Antenna Sub-array

Figure 6 (a) illustrates the configuration of the periodic slot antenna array with eight antenna elements. Each periodic slot array element is composed of rectangular-ring slots with different sizes connected together. Each rectangular slot could play as a resonator to change the antenna impedance matching and lead to bandwidth improvement. The S parameters of the sub-array are represented in Fig. 6 (b). As illustrated, the antenna elements provide very wide bandwidth in the mm-wave frequency range. Good impedance matching and high isolation characteristics are achieved for the sub-array. The worst coupling of the elements is <-25 dB within the operating bands.

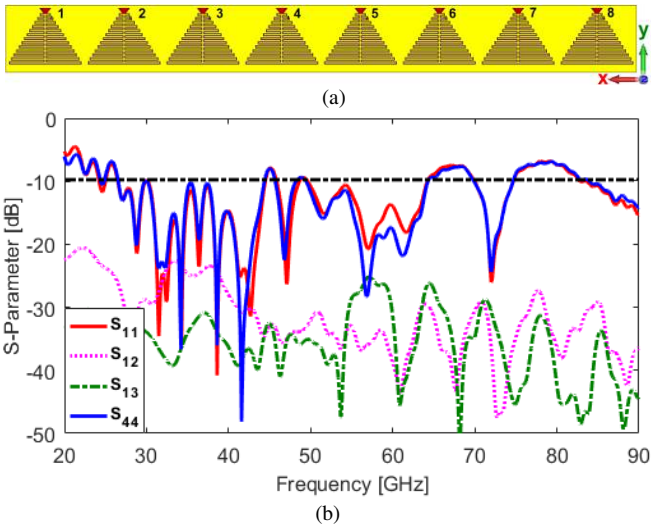

Fig. 6. (a) Periodic slot antenna array and its (b) S parameters.

The surface current distributions of the slot antenna at different frequencies are analyzed and illustrated in Fig. 7. It can be observed at the lower frequencies (especially at 30 GHz) the current concentrated around of the bigger rectangular slots. By increasing the operation frequency, as shown, the current flows more dominant around the small rectangular slots. All these are mainly because of the length of each radiator. As an example, it can be observed in Fig. 7 (f) that the current flows are fairly stronger at the upper slots while they are much weaker at the bigger slots, which reveals that each rectangular slot provides new resonance related to the radiator lengths. Accordingly, the impedance of the antenna changes at different frequencies due to the resonant function for the length of connected rectangular slot structures [27].

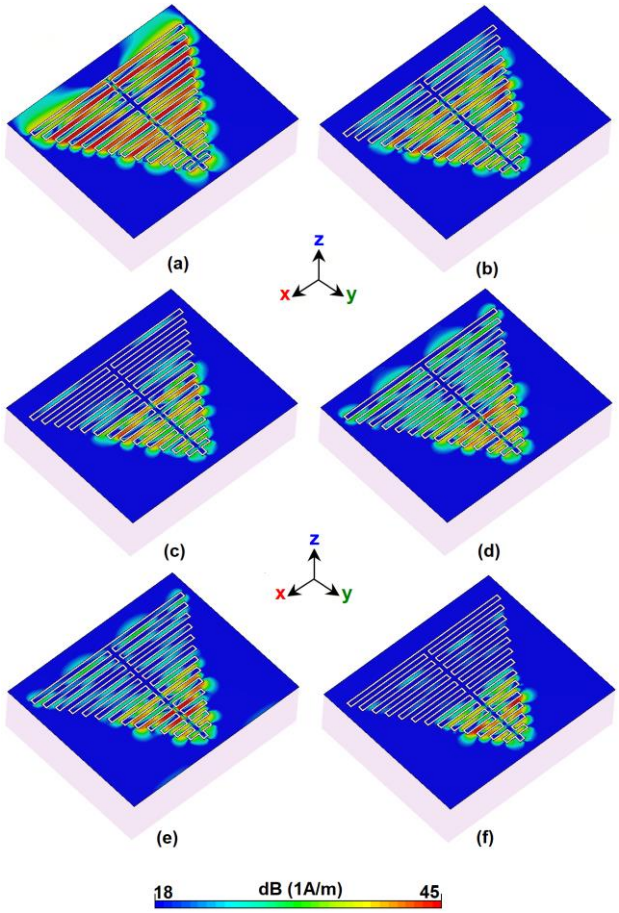

Fig. 7. Surface current distributions at (a) 30 GHz, (b) 40 GHz, (c) 50 GHz, (d) 60 GHz, (e) 65 GHz, and (f) 75 GHz.

The proposed planar periodic slot antennas are vertically polarized with the horizontal placement on the edge of a pure copper plate. This can be explained as follows: As we know, a periodic dipole antenna is horizontally polarized in the end-fire direction. The periodic slot antenna (designed in this paper) is a complementary structure of a periodic dipole antenna. According to Babinet's principle, the fields of the periodic slot antenna are similar to the periodic dipole antenna but their field's components (electric and magnetic fields) are interchanged. Therefore, for a horizontal periodic slot antenna, the polarization of the produced radiation is vertical [28].

The quasi end-fire radiation patterns are obtained mainly due to the existence of the substrate loaded under one side of the copper layer. In order to understand the phenomenon behind this, the electric and magnetic (E & H) field distributions at 33 GHz (central frequency) for the slot antenna element with and without substrate are illustrated in Figs. 8 (a) and (b), respectively. The cut planes for the vector E-field and H-field are placed between the copper-ground edge and the periodic-slot tip. For the antenna without substrate, the E-fields (and H-fields) on both sides of the copper layer have the same

amplitude but are out of phase. Therefore, as shown in Fig. 8 (c), the radiation pattern would have a null due to the field cancelation in the exact end-fire direction (90°). By employing a thick substrate on one side of the copper plate, most of the field/energy is constrained in the substrate side. This leads to much stronger E- and H-fields in the copper layer side loaded by the substrate than those in the side without the dielectric, though the E-fields (and H-fields) on both sides are still out of phase. The field cancelation in the end-fire direction is suppressed, and thus the end-fire radiation is enhanced with vertical polarization, as shown in Fig. 8 (c).

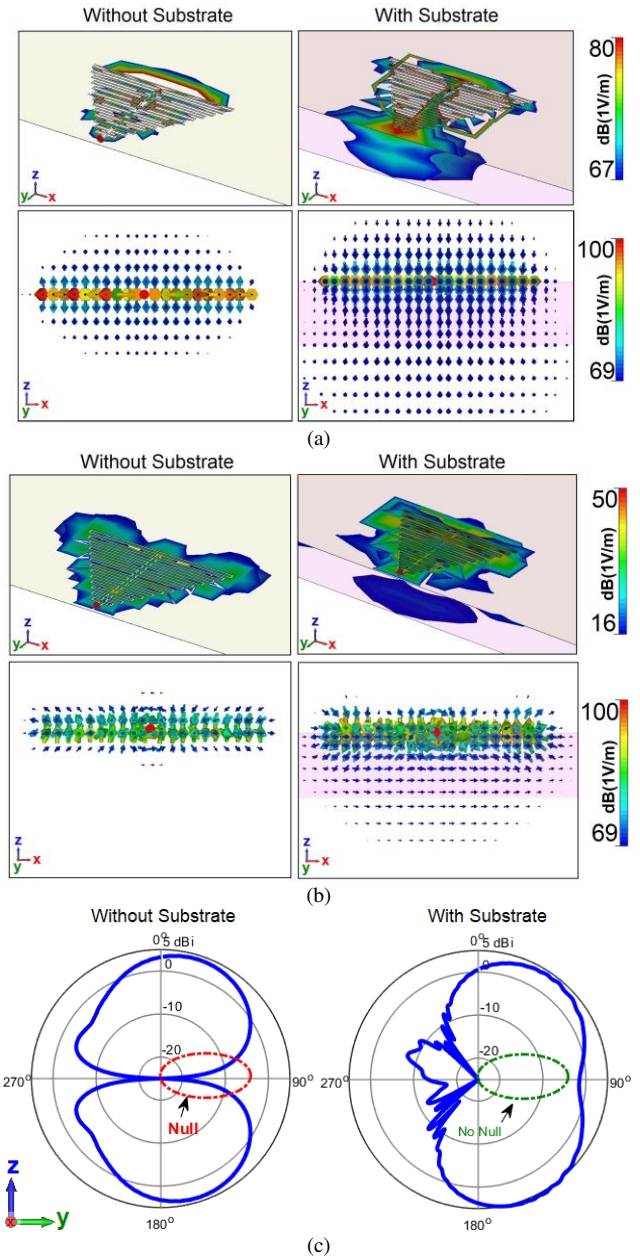

Fig. 8. (a) E-field, (b) H-field, and (c) 2D polar radiation patterns of the single element slot antenna without and with the employed substrate.

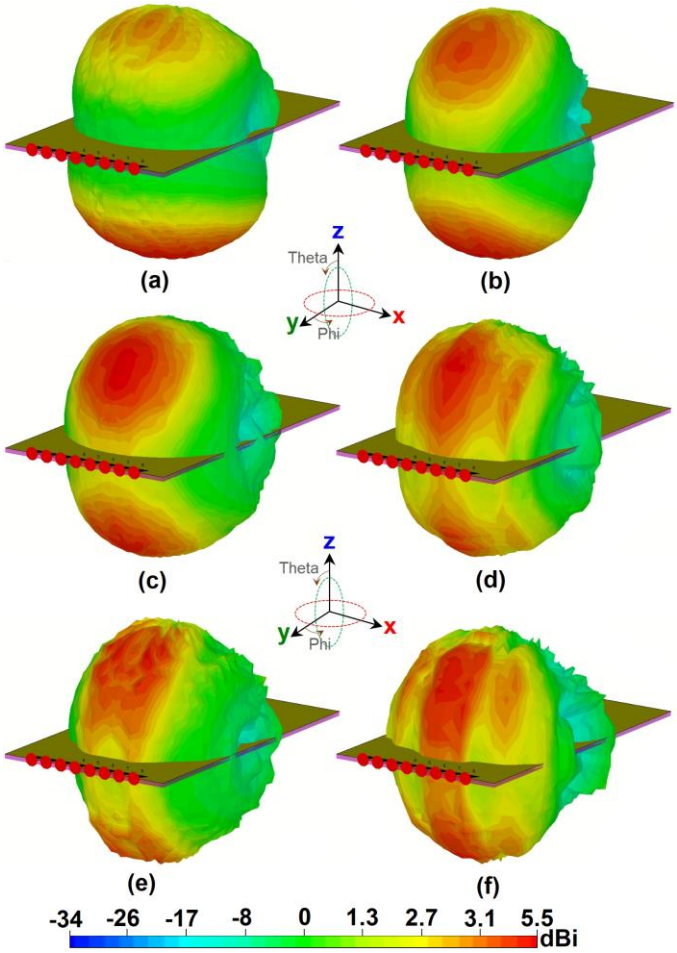

Fig. 9. Radiation patterns at (a) 30 GHz, (b) 40 GHz, (c) 50 GHz, (d) 60 GHz, (e) 65 GHz, and (f) 75 GHz.

Figure 9 depicts the radiation patterns of the single element CPW-fed periodic slot antenna employed at the top of the mobile phone PCB for the frequency range of 30-80 GHz. It should be noted that the color scale of the figure's label is non-linear (logarithmic). As can be found, the antenna provides quasi end-fire radiation patterns at different frequencies which is suitable for 5G mobile applications. Compared with other end-fire antennas such as Vivaldi, linearly-tapered slot antenna (LTSA), dipole, and Yagi antennas, the periodic slot antenna provides vertical polarization. This is the main advantage of the proposed design since it is difficult to achieve vertical polarization for the planar structures.

The antenna elements of the proposed beam-steerable slot array exhibit sufficient efficiencies over its ultra-wide bandwidth. As can be observed from Fig. 10, the element achieves -2~-0.5 dB (60~90%) radiation and total efficiencies versus its frequency band. Furthermore, as seen, the antenna element provides a high maximum gain with a value of 4~7.5 dBi over its operation band from 26.5 to 90 GHz.

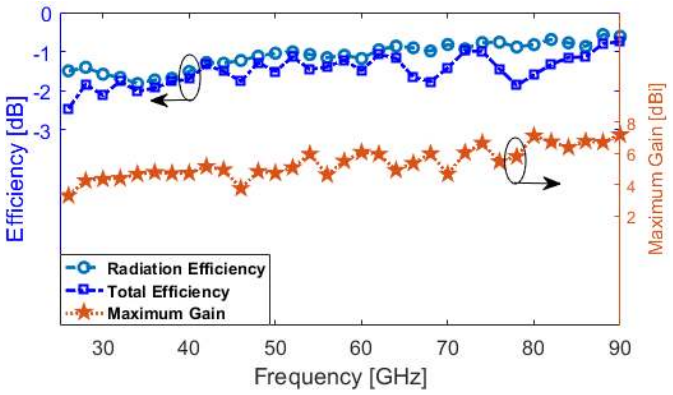

Fig. 10. Radiation properties of the slot antenna element versus its operation band.

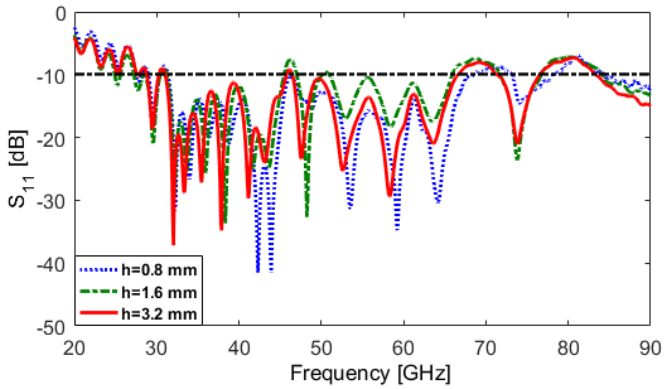

Fig. 11. Return loss characteristic of the slot element for different values of h_{sub}.

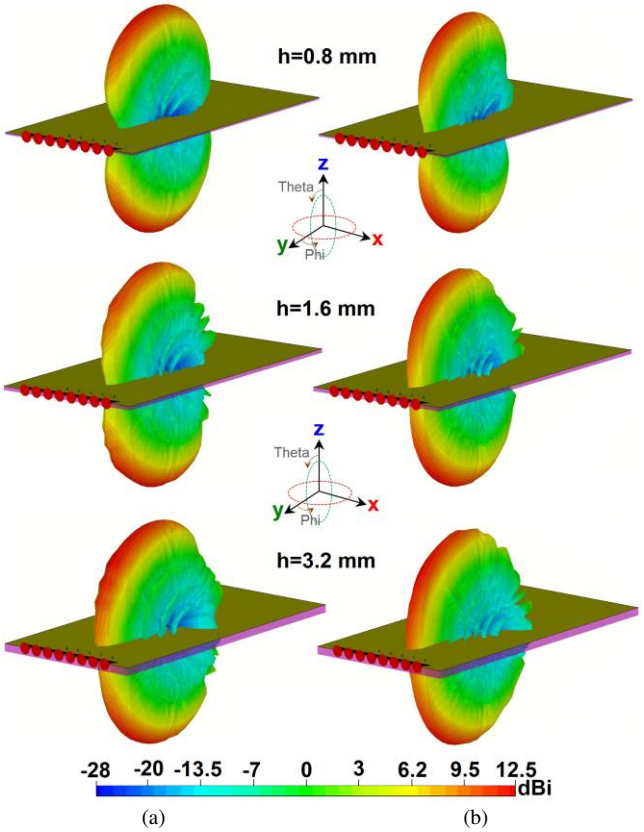

(a) (b)

Fig. 12. Radiation beams of the slot array at (a) 28 GHz and (b) 38 GHz for different values of h_{sub}.

It should be noted that the reflection coefficient characteristic of the antenna element is almost insensitive for different values of the substrate thickness. Figure 11 illustrates the reflection coefficients of the slot antenna with the substrate thickness of 0.8, 1.6, and 3.2 mm. The permittivity of the employed substrate is 2.3. As seen, there is no significant difference between the impedance matching of the antenna with different substrate thicknesses. However, in contrast with this characteristic, the radiation in end-fire is highly dependent on the substrate thickness. Based on the results in Fig. 12, the antenna array with a thicker substrate provides better end-fire radiation beams. As shown, the antenna with h=3.2 mm could provide much better end-fire beams in comparison with the antenna with a thinner substrate. So, a trade-off between the end-fire mode and PCB thickness is needed. For the proposed 5G array design, the thickness of the substrate is 1.575 mm.

C. Radiation Performance of the Proposed Dual-Polarized 5G Antenna Array

Figure 13 (a) depicts the configuration of the proposed planar dual-polarized array antenna. The design consists of two sub-arrays including 8-element CPW-fed dipole antennas with horizontally-polarized beams and vertically-polarized CPW-fed periodic slot antenna elements employed on the PCB ground plane of the 5G mobile platform. The distance between the vertically/horizontally polarized elements is 6.6 mm which is larger than λ/2 of the centre frequency of the operation band which might not be good enough for the large scanning purpose. This is mainly due to the dual-polarized function of the design in which unlike the single (linearly) polarized array, for the chosen d (element-to-element distance), instead of one element, two (slot/dipole) elements are placed. Reflection coefficient and mutual coupling characteristics of the CPW-fed dipole and slot antennas are represented in Fig. 13 (b). As shown, both antennas cover the 28 and 38 GHz 5G bands. In addition, the mutual coupling between two polarizations is less than -14 dB which is desirable for phased array applications.

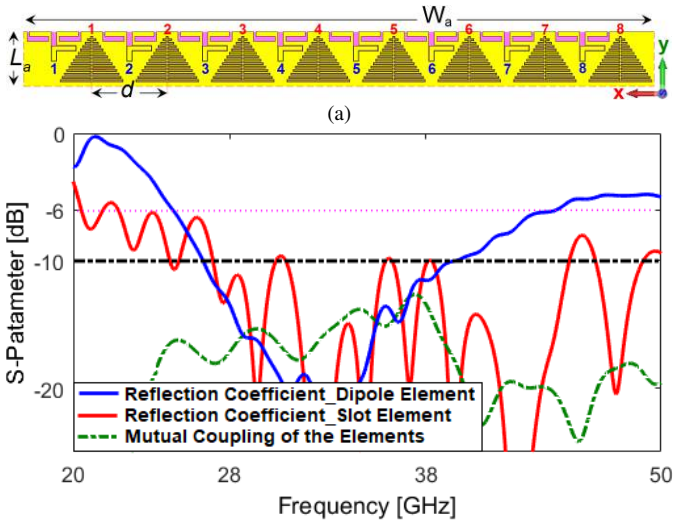

(a) (b)

Fig. 13. (a) Configuration and (b) S-parameters of the proposed CPW-fed array.

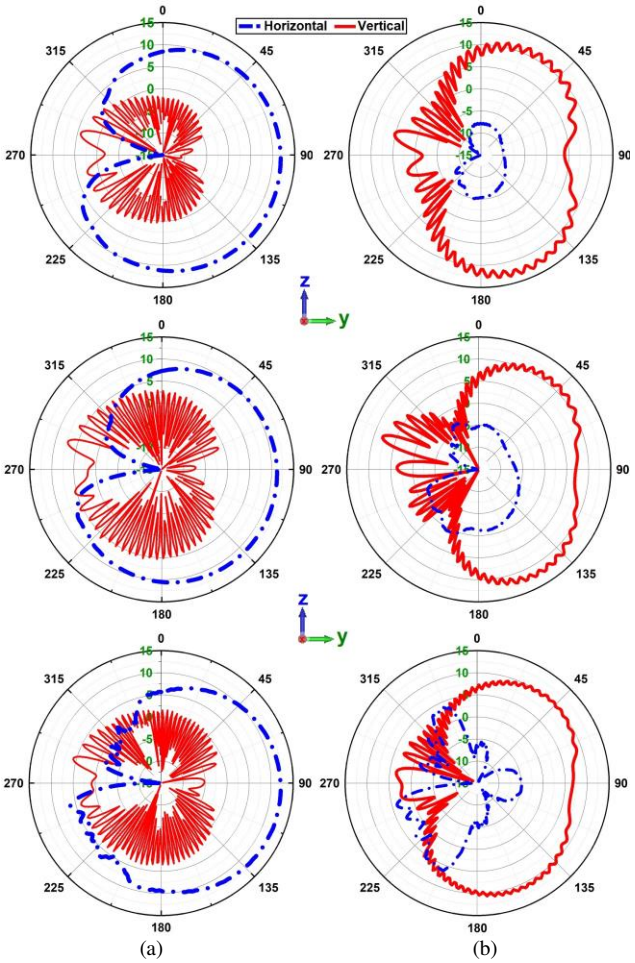

Fig. 14. (a) Horizontally-polarized and (b) vertically-polarized radiation beams of the array at different frequencies.

Figure 14 illustrates the horizontal and vertical polarized radiation beams of the array with realized gain values in 2D-polar views. It can be observed that the periodic slot sub-array provides quasi end-fire radiation beams with vertical polarization, while the horizontally polarized radiation beams have been achieved by the dipole radiators.

IV. Measurement Results and Discussions

The proposed 5G mobile-phone design has been properly fabricated and the characteristics of the antenna elements have been measured. Many challenges were faced during the fabrication and measurements of the proposed design. This can be mainly due to the compact size of the antenna radiators and also the employed feeding mechanism of the design. In order to measure the performances of the antenna elements, as shown in Fig. 15 (a), coaxial cables were used for the feeding (the inner-conductor of the coaxial cable is extended between the feeding points). The fabricated prototype of the proposed design is shown in Fig. 15 (b).

Figure 16 depicts the measured and simulated reflection coefficient (S_{nn}) of the radiation elements located at the edge and middle of the proposed antenna array. A slight variation in the measured S-parameters of the prototype was confirmed which can be due to the connectors, feeding setup, and the large length of the employed cables. In addition, the antenna elements are highly miniaturized and the slot-gap for the radiators of the prototype is 0.05 mm. However, for $S_{11} \leq -6$ dB, sufficient results have been obtained to cover 28 and 38 GHz 5G bands. The measured antenna elements provide a broad impedance bandwidth, covering the frequency range of 25 to 45 GHz. It should be noted that in all the measured results, the losses from the cables and connectors are not included. The far-field radiation patterns of the single-element antennas at different frequencies have been also measured.

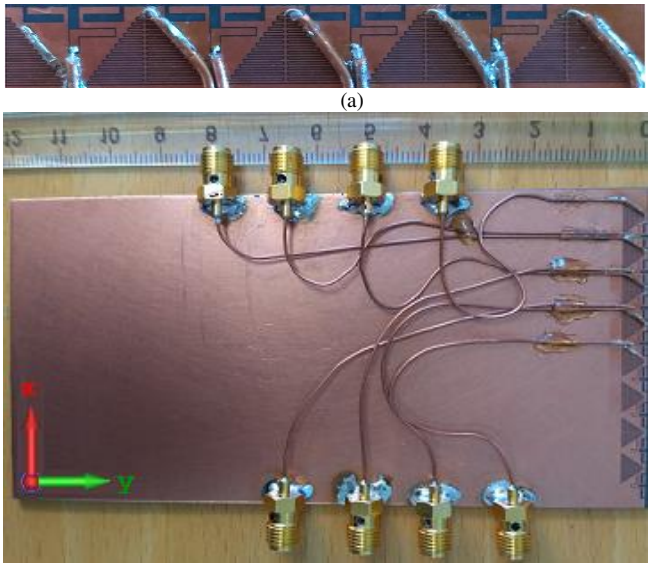

Fig. 15. (a) Feeding mechanism and (b) fabricated prototype of the proposed array design.

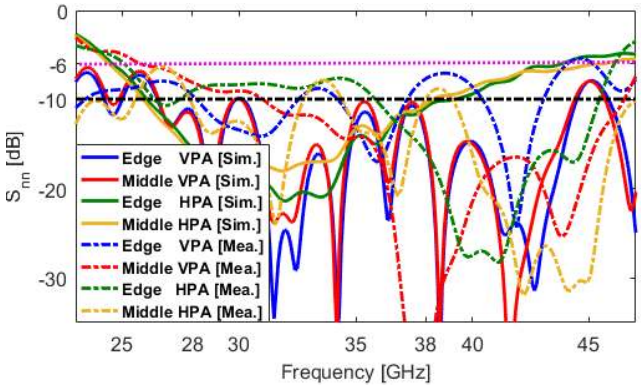

Fig. 16. Measured and simulated S_{nn} results of the antenna elements.

Figure 17 shows the measurement setup for antenna radiation patterns in the Anechoic Chamber. Figures 18 and 19 illustrate and compare the measured and simulated 2D polar radiation patterns for the dipole and slot antenna elements, respectively. 28, 33, and 36 GHz were selected to cover the lower, middle, and upper frequencies of the operation bands. It should be noted due to the discordant measured radiation pattern of the dipole element in 38 GHz, the radiation pattern results at 36 GHz are discussed instead, for the upper frequency of both antenna elements. As illustrated, both antenna elements can provide quasi end-fire radiation patterns with good consistency at different frequencies. In the figures, all the scale numbers are placed on the right side of the corresponding grid circles for each subfigure. The dynamic range is from -25 to 5

dBi, where the number of -25 dBi will be on the origin and not marked in the figure. The radiation's main direction ended in H-plane, as expected for end-fire modes. As seen, the shape of the radiation patterns in simulations and measurements is similar, especially in H-plane. Therefore, a generally good agreement is observed between the simulated and radiation patterns for both dipole and slot antenna elements in H and E planes.

Fig. 17. Measurement setup for the radiation patterns.

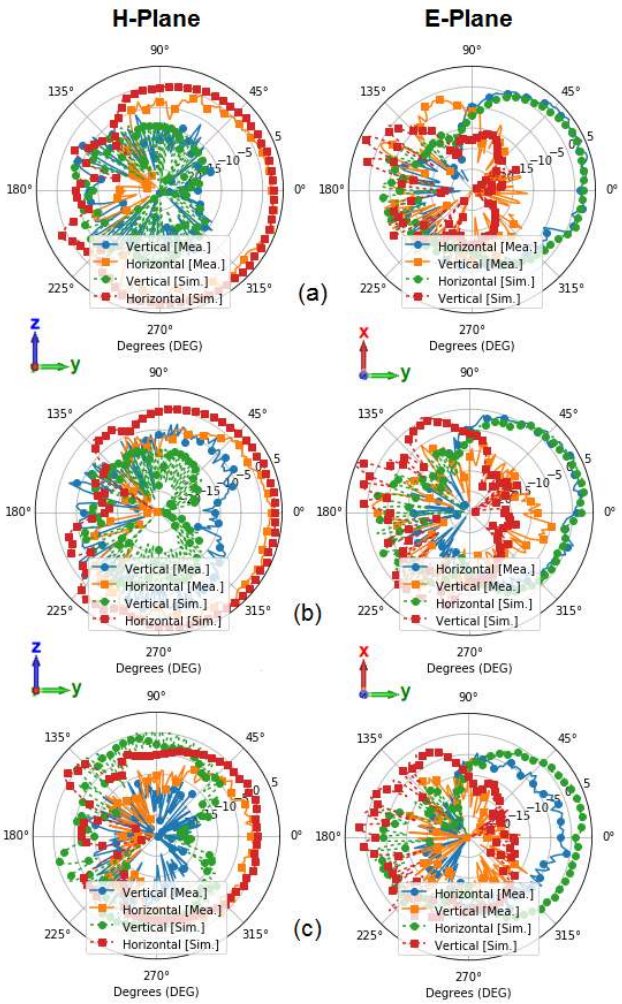

Fig. 18. Comparison of the measured and simulated radiation patterns of the dipole antenna element at, (a) 28 GHz, (b) 33 GHz, and (c) 36 GHz.

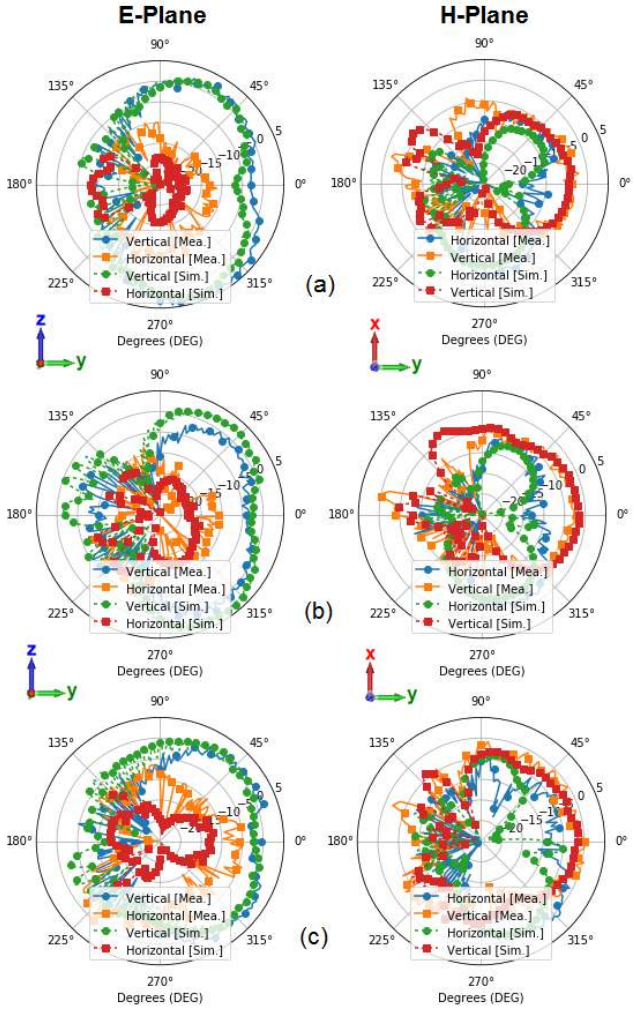

Fig. 19. Comparison of the measured and simulated radiation patterns of the slot antenna element at, (a) 28 GHz, (b) 33 GHz, and (c) 36 GHz.

However, a slight discrepancy is seen in E-plane which could be due to possible sources errors discussed previously along with the mutual coupling effects of the adjacent elements, since the measurement and simulation setups of the proposed antenna were not exactly the same. Furthermore, as can be observed, the peak realized gain of the elements was around 5 dBi realized gain, especially at 28 GHz. It has been slightly decreased as the frequency increased.

V. Conclusion

A new and compact design of a dual-polarized antenna array for mm-wave 5G cellular applications has been presented in this manuscript. The configuration of the proposed dual-polarized array structure contains two planar end-fire sub-arrays with different polarization (horizontal/vertical). Both of the sub-arrays can cover 28 and 38 GHz bands and provide sufficient properties in terms of impedance matching, gain, efficiency, directivity, and beam-coverage. The employed dual-polarized array has a compact size printed on one-layer of the substrate. These advantages make the proposed dual-polarized antenna array highly suitable for use in 5G mobile communications.

REFERENCES

[1] A. Osseiran, *et al.*, "Scenarios for 5G mobile and wireless communications: the vision of the METIS project," *IEEE Commun. Mag.,* vol. 52, pp. 26-35, 2014.

[2] W. Roh, *et al.*, "Millimeter-wave beamforming as an enabling technology for 5G cellular communications: Theoretical feasibility and prototype results," *IEEE Commun. Mag.*, vol. 52, pp. 106–113, 2014.

[3] W. Hong, K. Baek, and S. Ko, "Millimeter-wave 5G antennas for smartphones: Overview and experimental demonstration," *IEEE Trans. Antennas Propag.,* vol. 65, no. 12, pp. 6250–6261, 2017.

[4] S. Zhang, I. Syrytsin, G.F. Pedersen, "Compact beam-steerable antenna array with two passive parasitic elements for 5G mobile terminals at 28 GHz," *IEEE Trans. Antennas Propag.*, vol. 66, pp. 5193-5203, 2018.

[5] M.M.S. Taheri, A. Abdipour, S. Zhang, G.F. Pedersen, "Integrated millimeter-wave wideband end-fire 5G beam steerable array and low-frequency 4G LTE antenna in mobile terminals," *IEEE Trans. Veh. Technol.*, vol. 68, pp. 4042-4046, 2019.

[6] Y. Cai, , Y.-S. Zhang, , Z.-P. Qian, , W.-Q. Cao, , and S.-J. Shi, "Compact wideband dual circularly polarized substrate integrated waveguide horn antenna," *IEEE Trans. Antennas Propag.*, vol. 64, pp. 3184–3189, 2016.

[7] S.-T. Liu, Y.-W. Hsu, Y.-C. Lin, "A dual polarized cavity-backed aperture antenna for 5G mmW MIMO applications," *IEEE International Conference on Microwaves, Communications, Antennas and Electronic Systems (COMCAS)*, Tel Aviv, Israel, 2015.

[8] Y. Cai, Y.-S. Zhang, Z.-P. Qian, W.-Q. Cao, S.-J. Shi, "Compact wideband dual circularly polarized substrate integrated waveguide horn antenna," *IEEE Trans. Antennas Propag.*, vol. 64, pp. 3184–3189, 2016.

[9] Y.-S. Zhang, Y. Cai, N. Jing, Z.-P. Qian, S.-J. Shi, "Design of millimeter-wave dual circularly polarized end-fire antenna fed by SIW polarizer," *2016 IEEE MTT-S Int. Microwave Workshop Series on Advanced Materials and Processes for EF and THz Applications (IMWS-AMP)*, Chengdu, China, July 2016

[10] S. Wu, A. Zhao, Z. Ren, "Dual-polarized ring-slot 5G millimeter-wave antenna and array based on metal frame for mobile phone applications," *2019 13th European Conference on Antennas and Propagation (EuCAP)*, 31 March-5 April 2019, Krakow, Poland.

[11] W. Hong, S.-T. Ko, Y. Lee, K.-H. Baek, "Compact 28 GHz antenna array with full polarization flexibility under yaw, pitch, roll motions," *2015 9th European Conference on Antennas and Propagation (EuCAP),* 13-17 April 2015, Lisbon, Portugal.

[12] J. Park, D. Choi, W. Hong, "28 GHz 5G dual-polarized end-fire antenna with electrically-small profile," *12th European Conference on Antennas and Propagation (EuCAP 2018)*, 9-13 April 2018, London, UK.

[13] W. Hong, K. H. Baek, and S. Ko, "Millimeter-wave 5G antennas for smartphones: Overview and experimental demonstration," *IEEE Trans. Antennas Propag.*, vol. 65, no. 12, pp. 6250–6261, Dec. 2017.

[14] O. Jo *et al*, "Exploitation of dual-polarization diversity for 5G millimeter-wave MIMO beamforming systems," *IEEE Trans. Antennas Propag.*, vol. 65, pp. 6646-6655, 2017.

[15] W. Hong, K. Baek, and Y. Lee. "Quantitative analysis of the effects of polarization and pattern reconfiguration for mmWave 5G mobile antenna prototypes," *in Proc. IEEE. Radio and Wireless Symp.*, pp. 68–71, 2017.

[16] N. O. Parchin, M. Shen, and G. F. Pedersen, "UWB mm-wave antenna array with quasi omnidirectional beams for 5G handheld devices," *IEEE International Conference on Ubiquitous Wireless Broadband (ICUWB)*, pp.5-8, 2016.

[17] C.D. Paola, S. Zhang, K. Zhao, Z. Yning, T. Bolin, and G.F. Pedersen, "Wideband beam-steerable array with hybrid high gain antennas for 5G mobile devices," *IEEE Trans. Antennas Propag.*, 2019, Accepted.

[18] Y.-W. Hsu, T.-C. Huang, H.-S. Lin, and Y.-C. Lin, "Dual-polarized quasi Yagi-Uda antennas with end-fire radiation for millimeter-wave MIMO terminals," *IEEE Trans. Antennas Propag.*, vol. 65, pp. 6282- 6289, 2017.

[19] A. Li, K.-M. Luk, and Y. Li, ''A dual linearly polarized end-fire antenna array for the 5G applications,'' *IEEE Access*, vol. 6, pp. 78276–78285, 2018.

[20] M. A. Basit, G. Wen, N. Rasool, X. Xiaolin, "A wide-band cavity-backed slot antenna for end-fire radiation," *Microwave and Optical Technology letters*, vo. 58, pp. 193-198, 2016.

[21] H. Kim and C. W. Jung, "Ultra-wideband endfire directional tapered slot antenna using CPW to wide-slot transition," *Electron. Lett.*, vol. 46, pp. 1183–1185, 2010.

[22] K. Kanjanasit, C. Wang, "A wideband resonant cavity antenna assembled using a micromachined CPW-fed patch source and a two-layer metamaterial superstrate," *IEEE Trans. Compon. Packag. Manuf. Technol.*, vol. 9, pp. 1142-1150, 2019.

[23] Hittite Microwave Company, "Analog phase shifter," HMC933LP4E.

[24] MA-COM Technol. Solutions Holding, Inc., "PIN diode switch," SP3TAlGaAs.

[25] Y. Huo, X. Dong, and W. Xu, "5G cellular user equipment: From theory to practical hardware design," *IEEE Access*, vol. 5, pp. 13992–14010, 2017.

[26] K. Zhao, *et al.*, "Spherical coverage characterization of 5G millimeter wave user equipment with 3GPP specifications," *IEEE Access*, vol. 7, pp. 4442–4452, 2019.

[27] A. U. Bhobe, C. L. Holloway, M. Piket-May, and R. Hall, "Wide-band slot antennas with CPW feed lines: Hybrid and log-periodic designs," *IEEE Trans. Antennas Propag.*, vol. 52, no. 10, pp. 2545–2554, Oct. 2004.

[28] C. A. Balanis, "*Antenna theory analysis and design-4th edition*," John Wiley & Sons, New York, 1998.